ELSEVIER

Journal of Alloys and Compounds 463 (2008) 533–538

Journal of ALLOYS AND COMPOUNDS

www.elsevier.com/locate/jallcom

Morphological, structural, and mechanical characterizations of InGaN thin films deposited by MOCVD

Ping-Feng Yang [a,b], Sheng-Rui Jian [c], Yi-Shao Lai [a], Chu-Shou Yang [d], Rong-Sheng Chen [b,*]

[a] *Central Labs, Advanced Semiconductor Engineering Inc., 26 Chin 3rd Road, Nantze Export Processing Zone, Nantze, 811 Kaohsiung, Taiwan*
[b] *Department of Engineering Science, National Cheng Kung University, 701 Tainan, Taiwan*
[c] *Department of Materials Science and Engineering, I-Shou University, 840 Kaohsiung, Taiwan*
[d] *Department of Electrophysics, National Chiao Tung University, 300 Hsinchu, Taiwan*

Received 23 May 2007; received in revised form 20 September 2007; accepted 21 September 2007
Available online 12 October 2007

Abstract

Presented in this study are surface roughness, crystalline structure, and nanomechanical properties of InGaN thin films deposited under various growth temperatures, obtained by means of X-ray diffraction (XRD), atomic force microscopy (AFM), and nanoindentation techniques. The InGaN thin films with different In contents were deposited on sapphire substrates through a metal-organic chemical-vapor deposition (MOCVD) system. Changes in mechanical properties for InGaN thin films are discussed in conjunction with deposition temperature, surface morphology and crystalline structure. The XRD measurements showed that there was no phase separation of In as the In composition went from 25 at.% to 34 at.%. Moreover, both XRD and AFM showed larger grain and surface roughness in $In_{0.25}Ga_{0.75}N$ thin films. Nanoindentation results indicate that hardness and Young's modulus both decreased as the indentation depth increased. The contact stress–strain relationships were also analyzed.
© 2007 Elsevier B.V. All rights reserved.

Keywords: InGaN; MOCVD; XRD; AFM; Nanoindentation

1. Introduction

Wide-band-gap GaN and related III-nitride materials have been attracting lots of attention for their technologically important applications in optical and electronic devices [1–4]. The (Al, In)GaN alloys, consisting of AlN, GaN, and InN, cover the entire visual spectrum up to UV. Till now, only the InGaN layers have been used in commercialized applications for group III-nitride based light emitting devices (LEDs) because of the difficulties in fabricating highly efficient LEDs using (Al)GaN layers. In the previous studies [5,6], the recombination mechanisms and emission properties for InGaN-based structures had been widely investigated. In contrast, research on the mechanical properties has not drawn an equal attention. Therefore, mechanical characterizations of materials in a nanometer-scale and the correlation with the microstructures are very important in recognizing their tribological behaviors.

Various methods have been developed for measuring the mechanical properties of thin films, such as Brillouin light scattering [7], impulse acoustic method [8], and atomic force microscopy (AFM) [9]. Among these methods, the nanoindentation technique plays a key role in understanding nanomechanical properties of thin films. Nanoindentation has been proven to be a powerful technique in providing information on mechanical properties (hardness and elastic modulus) of the investigated materials and variation of these properties with the penetration depth based on analysis of the load–displacement curves [10–19]. The most important advantage of nanoindentation is to obtain, nondestructively, the films properties without being affected by its substrate. This method permits the evaluation of structural deformations of thin films in a nanometer-scale. These were and still are believed to primarily govern some aspects of the contact performance of materials adopted in most surface engineering and tribological applications. Consequently, measurements and knowledge of these surface-related properties are of prime importance for practical applications of various systems in various environments.

In recent years, the nanoindentation-induced plastic behaviors and mechanisms of III–V semiconductor materials have

* Corresponding author. Tel.: +886 6275 7575x63328; fax: +886 6276 6549.
E-mail address: rschen@mail.ncku.edu.tw (R.-S. Chen).

0925-8388/$ – see front matter © 2007 Elsevier B.V. All rights reserved.
doi:10.1016/j.jallcom.2007.09.140

been discussed by Le Bourhis and Patriarche [20] using the AFM and the plane-view and cross-sectional transmission electron microscopy (TEM). To our best knowledge, at present, nanomechanical characterizations of InGaN thin films are still unavailable. Herein, the present study is therefore focused on nanomechanical characterizations of $In_xGa_{1-x}N$ thin films deposited by a metal-organic chemical-vapor deposition (MOCVD) system at various growth temperatures by using a nanoindentation technique. In addition, discussions of the indentation mechanisms of InGaN thin films in the nanometer-scale and the influence of the In content of the deposited films are presented.

2. Growth of InGaN films

2.1. Film growth conditions

The $In_xGa_{1-x}N$ thin films were grown in a horizontal low-pressure MOCVD reactor. The trimethylgallium (TMGa), trimethylindium (TMIn), and ammonia (NH_3) were used as source precursors for Ga, In, and N, respectively. Prior to the growth, the sapphire substrate was annealed to remove residual impurities on the surface in a H_2 ambient environment at 1120 °C for 10 min. A 25 nm thick GaN nucleation layer was first deposited onto the sapphire substrate at 520 °C for 4 min. The substrate temperature was then raised to 1120 °C to grow a nominally 2 μm undoped GaN layer. A 0.4 μm thick $In_xGa_{1-x}N$ thin film was then grown on top of the undoped GaN layer. During the growth of InGaN thin films, the reactor pressure, input NH_3, TMGa, and TMIn flow rates were kept at a constant 200 mbar and 12 slm, 26.5 μmol/min, and 25.5 μmol/min, respectively. The growth temperature varied from 730 °C to 790 °C to obtain InGaN films with various In contents.

2.2. Crystallographic characterizations

The crystallography of the deposited films was characterized using a Bede QC200 high-resolution X-ray diffraction (HRXRD) with Cu Kα irradiation at 40 kV and 0.4 mA. The In contents in these samples were evaluated by the separation between GaN and InGaN peaks in the XRD spectra [21], as shown in Fig. 1. The Vegard's law [21] along with XRD was employed by Chen et al. [22] and Zhou et al. [23] to determine the In content of $In_xGa_{1-x}N$. In the present study, In contents of the $In_xGa_{1-x}N$ thin films corresponding to growth temperatures of 790 °C, 760 °C, and 730 °C were 25%, 30%, and 34%, respectively. From the figure, broad InGaN peaks were due to the combined results of alloying, finite domain size effects, and inhomogeneous material [24]. No evidence of phase separation could be found as the In content increased, indicating that structurally high-quality InGaN films were obtained. Using Scherrer's formula [25], estimated grain sizes of $In_{0.25}Ga_{0.75}N$, $In_{0.3}Ga_{0.7}N$, and $In_{0.34}Ga_{0.66}N$ thin films were 9.92 nm, 9.84 nm, and 8.62 nm, respectively.

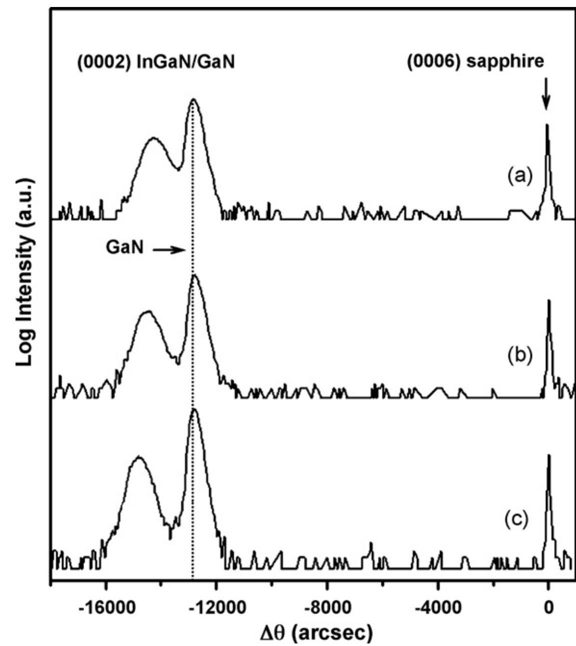

Fig. 1. XRD spectra of (a) $In_{0.25}Ga_{0.75}N$, (b) $In_{0.3}Ga_{0.7}N$, and (c) $In_{0.34}Ga_{0.66}N$ thin films.

2.3. Surface roughness characterizations

A Veeco/TM CP-R atomic force microscopy (AFM) was used to measure surface profiles of the samples. For the AFM operation, a constant load of 30 nN was applied to the cantilever and a constant scan speed of 1 μm/s was followed.

The surface roughness can be represented by centerline average (R_a) and root-mean-square average (RMS) [26] in the following forms:

$$R_a = \frac{1}{n}\sum_{i=1}^{n}|z_i|, \quad (1)$$

$$\mathrm{RMS} = \sqrt{\frac{1}{n}\sum_{i=1}^{n}z_i^2}. \quad (2)$$

The centerline is the line that divides the profile in such a way such that the net deviation is zero. Both R_a and RMS measure the average vertical deviation of the surface profile from the centerline. It should be noted that these parameters can only be used to compare surfaces generated by the same method [27].

Typical AFM images of $In_{0.25}Ga_{0.75}N$, $In_{0.3}Ga_{0.7}N$, and $In_{0.34}Ga_{0.66}N$ thin films deposited at growth temperatures of 790 °C, 760 °C, and 730 °C are presented in Fig. 2, in which island-like surfaces are clearly visible. Increase of the growth temperature enhances the mobility of atoms on the surface and hence increases grain size and surface roughness, which is clearly observed in the figure. The R_a and RMS of $In_{0.25}Ga_{0.75}N$, $In_{0.3}Ga_{0.7}N$, and $In_{0.34}Ga_{0.66}N$ thin films were summarized in Table 1 and compared to those of other III-nitride thin films [13,27].

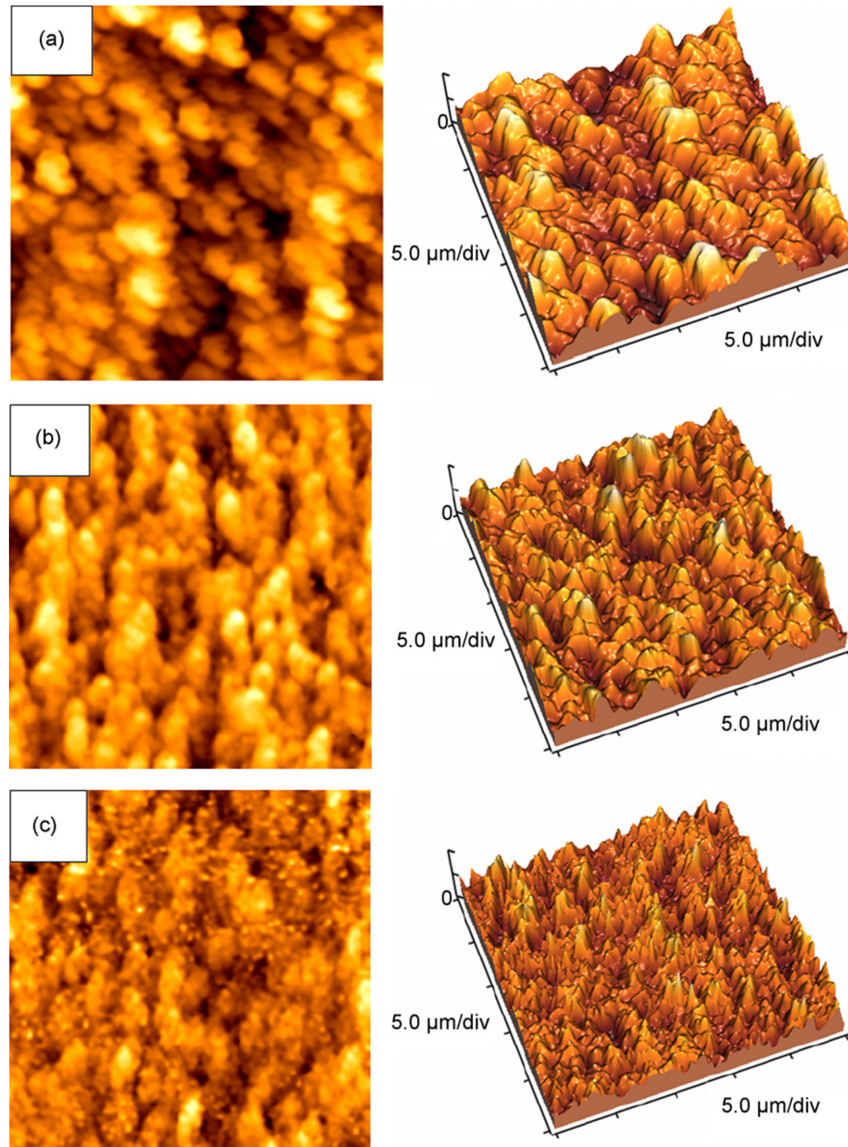

Fig. 2. 2D and 3D AFM images of (a) $In_{0.25}Ga_{0.75}N$, (b) $In_{0.3}Ga_{0.7}N$, and (c) $In_{0.34}Ga_{0.66}N$ thin films.

3. Nanoindentation

Hardness and elastic modulus of the thin films were calculated from the load–displacement data obtained by a nanoindenter (Triboscope, Hysitron Inc., USA). This apparatus monitors and records dynamic loads and displacements of a three-sided pyramidal Berkovich indenter during nanoindentation with a force resolution of about 50 nN and a displacement resolution of about 0.1 nm. The Berkovich shape has a half angle of 65.3° and a tip radius of 50 nm. Load-controlled indentation

Table 1
Structural, surface roughness, and mechanical properties of III-nitride thin films

Materials	R_a (nm)	RMS (nm)	D (nm)	H (GPa)	E_f (GPa)	τ_{max} (GPa)
GaN [13]	–	–	–	19.34 ± 2.13	314.93 ± 40.58	2.98 ± 0.11[a]
GaN:Si [13]	–	–	–	20.12 ± 2.51	247.16 ± 14.89	2.42 ± 0.13[a]
$Al_{0.12}Ga_{0.88}N$ [13]	–	–	–	19.24 ± 4.76	315.23 ± 43.09	2.98 ± 0.49[a]
$Al_xGa_{1-x}N$ ($0.09 < x < 0.27$) [27]	–	–	–	∼19.7 ± 0.4	∼375 ± 12	∼6.7 ± 1.4[a]
$In_{0.25}Ga_{0.75}N$[b]	4.65 ± 0.24	5.34 ± 0.28	9.92 ± 0.31	16.65 ± 1.07	375.87 ± 23.10	61.98 ± 3.84
$In_{0.3}Ga_{0.7}N$[b]	2.42 ± 0.14	2.95 ± 0.18	9.84 ± 0.23	16.49 ± 0.99	322.36 ± 13.45	57.51 ± 2.33
$In_{0.34}Ga_{0.66}N$[b]	2.26 ± 0.16	2.68 ± 0.20	8.62 ± 0.27	16.06 ± 0.68	373.99 ± 28.62	68.03 ± 5.12

[a] Pop-in.
[b] Present work.

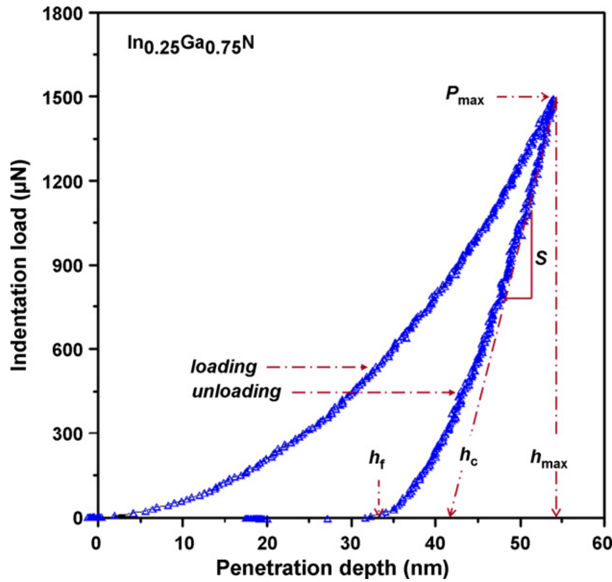

Fig. 3. Load–displacement curve of $In_{0.25}Ga_{0.75}N$ thin film for a maximum indentation load of 1500 μN.

testing followed a trapezoidal loading profile with a typical peak load hold time of 10 s. The peak loads ranged from 1000 μN to 2000 μN in a loading rate of 10 μN/s. A typical indentation experiment consisted of four subsequent steps: approaching the surface, loading to the peak load in a loading rate of 10 μN/s, holding the indenter at the peak load for 10 s, and completely unload. Holding was included to avoid the influence of creep on the unloading characteristics since the unloading curve was used to obtain the elastic modulus of the target material. Nanoindentation tests were performed when the thermal drift dropped down to 0.01 nm/s. The thermal drift effects were corrected for each test using a holding segment in the air before indentation. Ten indentations were made on each sample and the results presented are an average of these indentations.

The loading–unloading curve of $In_{0.25}Ga_{0.75}N$ thin film obtained for a maximum indentation load of 1500 μN is shown in Fig. 3, in which P_{max}, h_{max}, h_f, and h_C are denoted as the maximum indentation load, the maximum penetration depth, the residual depth, and the contact depth, respectively. Since the penetration depth did not exceed 20% of the film thickness [28], the substrate effect can be ignored. The slope of the unloading curve, S, stands for a measure of the stiffness. The contact stiffness can be expressed as [10,29]

$$S = \frac{dP}{dh} = 2\beta\frac{E_r A_C^{1/2}}{\pi^{1/2}}, \tag{3}$$

where E_r denotes the reduced elastic modulus and $\beta = 1.034$ is the shape constant for the Berkovich tip. The A_C is the projected contact area determined by h_{max}. For an ideal Berkovich indenter, $A_C = f(h_C) = 24.56h_C^2$, where $h_C = h_{max} - 0.72(P_{max}/S)$. The elastic modulus of the thin film, E_f, was calculated by

$$\frac{1}{E_r} = \frac{1-v_i^2}{E_i} + \frac{1-v_f^2}{E_f}, \tag{4}$$

where E and v are elastic modulus and Poisson's ratio, respectively, and subscripts i and f denote the indenter and thin film, respectively. For the diamond indenter, $E_i = 1141$ GPa and $v_i = 0.07$ [10]. We assume that $v_f = 0.3$. The hardness, H, is defined by

$$H = \frac{P_{max}}{A_C}. \tag{5}$$

From the loading–unloading curve, a plasticity index η that estimates the extent of plastic deformations induced by the nanoindentation process can be constructed as [30]

$$\eta = \frac{A_1}{A_1 + A_2}, \tag{6}$$

where A_1 is the area between loading and unloading curves and A_2 is the area between unloading curve and $P_{max} - h_{max}$ line. Hence $\eta = 1$ is referred to as a fully plastic deformation while $\eta = 0$ a fully elastic deformation. For $0 < \eta < 1$, the deformation is elastoplastic or elasto-viscoplastic. The η for $In_{0.25}Ga_{0.75}N$,

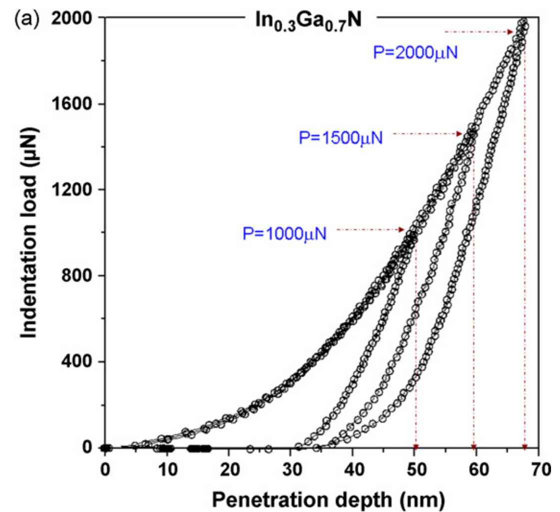

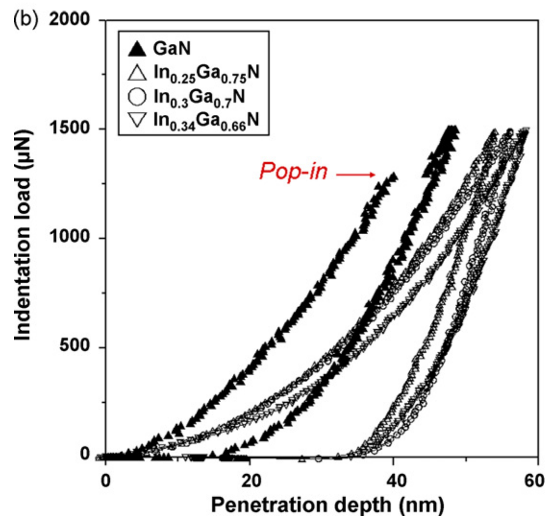

Fig. 4. Load–displacement curves for (a) $In_{0.3}Ga_{0.7}N$ thin film and (b) InGaN and GaN [13] thin films at an indentation load of 1500 μN.

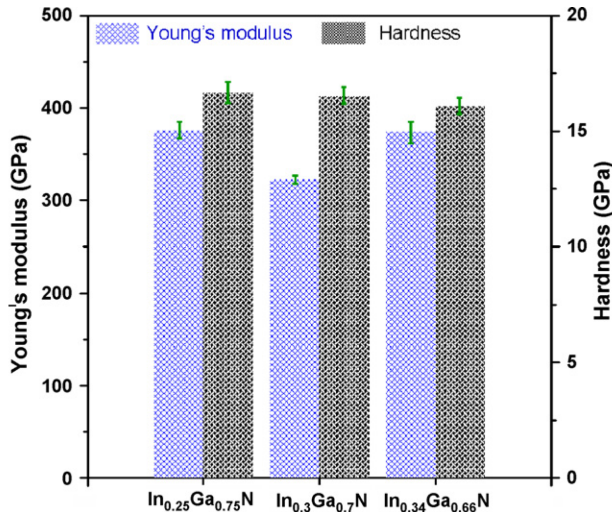

Fig. 5. Young's moduli and hardness of InGaN thin films.

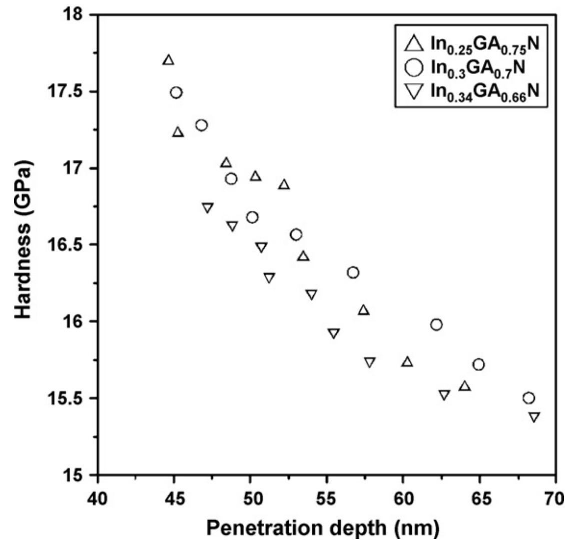

Fig. 6. Hardness as a function of penetration depth for InGaN thin films.

$In_{0.3}Ga_{0.7}N$, and $In_{0.34}Ga_{0.66}N$ thin films were found to be 0.58, 0.41, and 0.51, respectively.

Fig. 4(a) shows load–displacement curves obtained for $In_{0.3}Ga_{0.7}N$ thin films under maximum loads of 1000 μN to 2000 μN. These curves are smooth without discontinuities. As reported by Jian et al. [13], a "pop-in" event occurred during the loading stage for GaN thin films [13], as shown in Fig. 4(b), which suggests that preferential slips occurred after the nucleation of dislocations and up to the critical strain. This phenomenon has been attributed to the poor defect density inside the specimen prior to nanoindentation so that the onset of plasticity requires a load sufficient for nucleating and propagating dislocations. No such a pop-in event was found in load–displacement curves for InGaN thin films, however.

Along with geometry and elastic properties of the thin film, the maximum shear stress, $\tau_{\max}$, underneath the indenter tip can also be computed. The $\tau_{\max}$ below the indenter can be expressed through the mean contact pressure (p_a) from the Hertz contact theory [31]:

$$\tau_{\max} = 0.465 p_a = 0.47 \frac{16}{9} \frac{E_r^2 h_C^2}{\pi P_{\max}} = 0.465 \frac{4E_r}{3\pi} \sqrt{\frac{h_C}{R}} \quad (7)$$

The $\tau_{\max}$ of InGaN thin films, ranged from 57.51 ± 2.33 GPa to 68.03 ± 5.12 GPa, are also listed in Table 1.

As shown in Fig. 5, Young's moduli were 375.87 ± 23.10 GPa, 322.36 ± 13.45 GPa, and 373.99 ± 28.26 GPa for $In_{0.25}Ga_{0.75}N$, $In_{0.3}Ga_{0.7}N$, and $In_{0.34}Ga_{0.66}N$ thin films, respectively. Corresponding hardness were 16.65 ± 1.07 GPa, 16.49 ± 0.99 GPa, and 16.06 ± 0.68 GPa, respectively. For reference, the Young's modulus of GaN was found to be 314.93 ± 40.58 GPa [13]. Moreover, the hardness of $In_xGa_{1-x}N$ was lower than that of GaN, which is 19.34 ± 2.13 GPa [13], indicating that a greater In content leads to a lower hardness. In the previous section, we have shown that the InGaN thin film with a greater In content has a smaller grain size. Apparently, hardness of the thin film increases as its grain size increases, which coincides the characteristic reported by Wen et al. [32].

Nevertheless, as shown in Fig. 6, we need to point out that hardness decreases slightly as the indentation depth increases. This could be owing to the indentation size effect (ISE), for which the measured hardness increases as the indentation load decreases [33,34]. The ISE has been attributed to a variety of contributions, such as statistical measurements errors, dislocation nucleation, and surface and plastic strain energy dissipation [35–37].

Size effects in plastic deformed materials have been described in terms of strain gradient plasticity following the observation that plastic shear gradients produce storage of geometrically necessary dislocations [38]. As pointed out by Fleck and Hutchinson [39], this can be recognized by noting that the large strain gradients inherent in small indentations lead to geometrically necessary dislocations, which are related to the curvature of the crystal lattice and can cause enhanced hardening. Studies of the plastic response of materials subjected to the indentation have drawn an analogy between the plastic zone which expands radially beneath an indenter under the confinement of the neighboring elastic material and an expanding cavity [40]. At the dislocation level, this so-called expanding cavity model is visualized by a series of "geometrically necessary" prismatic dislocation loops that are punched out into the material to accommodate the indenter [41]. From experimental [42] and simulation [43,44] studies, the nucleation of dislocation causes microstructural transformations and slip bands on the surface of thin film.

Fig. 7 shows indentation contact stress–strain curves for InGaN thin films. The curves essentially represent elastic or elastoplastic behaviors of the thin films [11] by plotting the contact pressure against a contact strain, a_c/R, in which a_c denotes the radius of the contact area while R is the radius of the Berkovich tip. The a_c is determined based on Hertz contact [30] and the detailed calculations can be referred to Nowak et al. [11]. From the figure, it can be seen that the $In_{0.25}Ga_{0.75}N$ thin film features the largest contact stresses during the nanoindentation process.

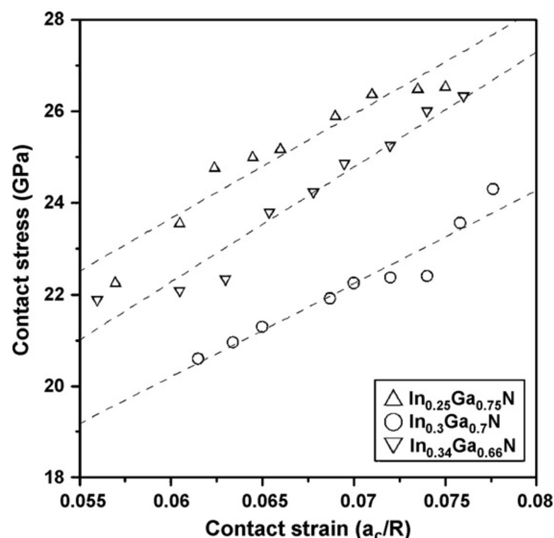

Fig. 7. Contact stress–strain relationships of InGaN thin films.

4. Conclusion

We report in this paper structural features and nanomechanical characterizations of InGaN thin films with different In contents generated by a MOCVD system using XRD, AFM, and nanoindentation techniques.

For $In_xGa_{1-x}N$ films with 25%, 30% and 34% In contents, XRD analysis showed no evidence of phase separation and AFM micrographs indicated relatively smooth surfaces. Through nanoindentation, Young's moduli of $In_{0.25}Ga_{0.75}N$, $In_{0.3}Ga_{0.7}N$, and $In_{0.34}Ga_{0.66}N$ thin films were found to be 375.87 ± 23.10 GPa, 322.36 ± 13.45 GPa, and 373.99 ± 28.26 GPa, respectively, while corresponding hardness were 16.65 ± 1.07 GPa, 16.49 ± 0.99 GPa, and 16.06 ± 0.68 GPa, respectively. The $In_{0.25}Ga_{0.75}N$ thin film features the largest contact stresses and strains during the nanoindentation process.

Acknowledgement

This work was partially supported by National Science Council of Taiwan through Grant NSC 96-2112-M-009-017.

References

[1] M.A. Khan, A. Bhattarai, J.N. Kuznia, D.T. Olson, Appl. Phys. Lett. 63 (1993) 1214–1215.
[2] S. Nakamura, M. Senoh, N. Iwasa, S. Nagahama, T. Yamada, T. Mukai, Jpn. J. Appl. Phys. 34 (1995) L1332–L1335.
[3] B. Gil (Ed.), Group III Nitride Semiconductor Compounds: Physics and Applications, Oxford University Press, New York, 1998.
[4] P. Kavouras, Ph. Komninoua, Th. Karakostas, Thin Solid Films 515 (2007) 3011–3018.
[5] S. Chichibu, T. Azuhata, T. Sota, S. Nakamura, Appl. Phys. Lett. 69 (1996) 4188–4190.
[6] Y. Narukawa, Y. Kawakami, S. Fujita, S. Fujita, S. Nakamura, Phys. Rev. B 55 (1997) R1938–R1941.
[7] P. Djemia, C. Dugautier, T. Chauveau, E. Dogheche, M.I. De Barros, L. Vandenbulcke, J. Appl. Phys. 90 (2001) 3771–3779.
[8] D.C. Hurley, V.K. Tewary, A.J. Richards, Thin Solid Films 398/399 (2001) 326–330.
[9] S. Chowdhury, M.T. Laugier, Nanotechnology 15 (2004) 1017–1022.
[10] W.C. Oliver, G.M. Pharr, J. Mater. Res. 7 (1992) 1564–1583.
[11] R. Nowak, M. Pessa, M. Suganuma, M. Leszczynski, I. Grzegory, S. Porowski, F. Yoshida, Appl. Phys. Lett. 75 (1999) 2070–2072.
[12] P. Papakonstantinou, P. Lemoine, J. McLaughlin, K. MacKay, P.M. Dodd, R.J. Pollard, R. Atkinson, J. Appl. Phys. 87 (2000) 6170–6172.
[13] S.-R. Jian, T.-H. Fang, D.-S. Chuu, J. Electron. Mater. 32 (2003) 496–500.
[14] B. Bhushan, X. Li, Int. Mater. Rev. 48 (2003) 125–164.
[15] C.-H. Chien, S.-R. Jian, C.-T. Wang, J.-Y. Juang, J.C. Huang, Y.-S. Lai, J. Phys. D: Appl. Phys. 40 (2007) 3985–3990.
[16] V.A. Coleman, J.E. Bradby, C. Jagadish, P. Munroe, Y.W. Heo, S.J. Pearton, D.P. Norton, M. Inoue, M. Yano, Appl. Phys. Lett. 86 (2005) 203105.
[17] R. Navamathavan, K.-K. Kim, D.-K. Hwang, S.-J. Park, T.G. Lee, G.-S. Kim, J.-H. Hahn, Mater. Lett. 61 (2007) 2443–2445.
[18] H. Yang, T. Yoshida, Surf. Coat. Technol. 200 (2005) 984–987.
[19] M. Fujikane, D. Setoyama, S. Nagao, R. Nowak, S. Yamanaka, J. Alloys Compd. 431 (2007) 250–255.
[20] E. Le Bourhis, G. Patriarche, Prog. Cryst. Growth Char. Mater. 47 (2003) 1–43.
[21] Z. Qin, Z. Chen, Y. Tong, S. Lu, G. Zhang, Appl. Phys. A 74 (2002) 655–658.
[22] Z.Z. Chen, Z.X. Qin, X.D. Hu, T.J. Yu, Z.J. Yang, Y.Z. Tong, X.M. Ding, G.Y. Zhang, Physica B 344 (2004) 292–296.
[23] S.Q. Zhou, M.F. Wu, L.N. Hou, S.D. Yao, H.J. Ma, R. Nie, Y.Z. Tong, Z.J. Yang, T.J. Yu, G.Y. Zhang, J. Cryst. Growth 263 (1994) 35–39.
[24] R.W. Vook, in: J.W. Matthews (Ed.), Epitaxial Growth, Part A, Academic Press, New York, 1975, p. 339.
[25] B.D. Cullity, Elements of X-ray Diffraction, 2nd ed., Addison–Wesley, Reading, MA, 1978.
[26] K. Miyoshi, Y.W. Chung, Surface Diagnostics in Tribology: Fundamental Principles and Applications, World Scientific Publishing, Singapore, 1993.
[27] D. Cáceres, I. Vergara, R. González, E. Monroy, F. Calle, E. Muñoz, F. Omnès, J. Appl. Phys. 86 (1999) 6773–6778.
[28] X. Wang, A. Kolitsch, W. Möller, Appl. Phys. Lett. 71 (1997) 1951–1953.
[29] G.M. Pharr, W.C. Oliver, F.R. Brotzen, J. Mater. Res. 7 (1992) 613–617.
[30] K.L. Johnson, Contact Mechanics, Cambridge University Press, Cambridge, 1985.
[31] D. Lorenz, A. Zeckzer, U. Hilpert, P. Grau, H. Johansen, H.S. Leipner, Phys. Rev. B 67 (2003) 172101.
[32] H. Wen, X. Wang, L. Li, J. Appl. Phys. 100 (2006) 084315.
[33] W.D. Nix, H. Gao, J. Mech. Phys. Solids 46 (1998) 411–425.
[34] A.A. Elmustafa, D.S. Stone, Acta Mater. 50 (2002) 3641–3650.
[35] W.W. Gerberich, N.I. Tymiak, J.C. Grunlan, M.F. Horstemeyer, M.I. Baskes, J. Appl. Mech. ASME 69 (2002) 433–442.
[36] N. Gane, J.M. Cox, Phil. Mag. 22 (1970) 881–891.
[37] F.G. Yost, Metall. Trans. A 14 (1983) 947–952.
[38] Q. Ma, D.R. Clarke, J. Mater. Res. 10 (1995) 853–863.
[39] N.A. Fleck, J.W. Hutchinson, J. Mech. Phys. Solids 49 (2001) 2245–2271.
[40] K.L. Johnson, J. Mech. Phys. Solids 18 (1970) 115–126.
[41] F. Seitz, Phys. Rev. 79 (1950) 723–724.
[42] J.E. Bradby, S.O. Kucheyev, J.S. Williams, J. Wong-Leung, M.V. Swain, P. Munroe, G. Li, M.R. Phillips, Appl. Phys. Lett. 80 (2002) 383–385.
[43] W.C.D. Cheong, L.C. Zhang, Nanotechnology 11 (2000) 173–180.
[44] J. Li, K.J. Van Vliet, T. Zhu, S. Yip, S. Suresh, Nature 418 (2002) 307–310.